Spectroelectrochemical Characterization of the [NiFe] Hydrogenase of *Desulfovibrio vulgaris* Miyazaki F[†]

Caroline Fichtner, Christoph Laurich, Eberhard Bothe, and Wolfgang Lubitz*

Max-Planck-Institut für Bioanorganische Chemie, Stiftstrasse 34-36, D-45470 Mülheim/Ruhr, Germany

Received February 6, 2006; Revised Manuscript Received May 22, 2006

ABSTRACT: The active site in the [NiFe] hydrogenase of *Desulfovibrio vulgaris* Miyazaki F has been investigated by Fourier transform infrared (FTIR) spectroscopy. Analysis of the spectra allowed the three diatomic inorganic ligands to Fe in this enzyme to be identified as one CO molecule and two CN^- molecules. Furthermore, pH-dependent redox titrations were performed to determine the midpoint potentials as well as the p*K* value of the respective reactions and revealed that each single-electron redox transition is accompanied by a single-proton transfer step. The comparison of these spectra with those published for other [NiFe] hydrogenases shows that the electronic structure of the active sites of these enzymes and their redox processes are essentially the same. Nevertheless, differences with respect to the frequency of the CO band and the pH dependence of the Ni-R states have been observed. Finally, the frequency shifts of the bands in the IR spectra were interpreted with respect to the electronic configuration of the redox intermediates in the catalytic cycle.

Hydrogenases are enzymes that catalyze the reversible oxidation of molecular hydrogen. They occur in a wide variety of microorganisms through all phylogenetic groups and play an important role in the metabolism by supporting the generation of a proton gradient across the cytoplasmic membrane and/or by generating reducing equivalents which are involved in metabolic processes (*1*). Hydrogenases are divided into different classes according to the metal content of the active site. Among those, the [NiFe] hydrogenases form the largest class. The [NiFe] hydrogenase of *Desulfovibrio vulgaris* Miyazaki F, a sulfate-reducing δ-proteobacterium, is a heterodimeric protein of 89 kDa (*2*) (see Figure 1). Its structure has been resolved to high resolution by X-ray crystallography in different redox states (*2*−*5*). The small subunit contains three [FeS] clusters that are involved in the electron transfer between the active site and the protein surface. The active site is deeply buried in the large subunit and contains one Ni atom and one Fe atom. The active site, including the amino acid surrounding, is shown in Figure 1b. The Ni atom is coordinated by four sulfur atoms of four cysteine residues. Two are terminally bound to Ni (Cys546 and Cys81), and the other two form a bridge between Ni and Fe (Cys549 and Cys84) (*2*). Furthermore, the Fe is ligated by three diatomic inorganic ligands. These ligands were initially modeled as one CO molecule, one CN^- molecule, and one SO molecule in the X-ray structure (*2*), which differs from the identification by infrared spectroscopy of these ligands in the closely related hydrogenases of *Desulfovibrio gigas* and *Allochromatium vinosum* where two CN^- molecules and one CO molecule were found (*6*). In a more recent X-ray analysis of the *D. vulgaris* Miyazaki F enzyme, these molecules were found to be more compatible with two CO molecules and one CN^- molecule (*5*).

A third bridging position between Ni and Fe is present which is occupied by different ligands during the catalytic reaction. The intermediate states of the active center differ in their redox and spectroscopic properties. In the most oxidized form of the [NiFe] center, two redox states called Ni-A (the "unready" state) and Ni-B (the "ready" state) coexist . Both states are catalytically inactive and differ in the time needed for activation (*7*). For Ni-B, the bridging ligand has been identified by single-crystal EPR[1] spectroscopy as a OH^- group (*8*−*10*). In case of Ni-A, a diatomic oxygen species is proposed (*5*, *8*, *11*). The enzyme is activated under reducing conditions and passes through the Ni-SU, Ni-SI, Ni-C, and Ni-R states, where Ni-SU is the one-electron-reduced state of Ni-A, Ni-SI is the one-electron-reduced state of Ni-B, and Ni-C and Ni-R are the one- and two-electron-reduced states of Ni-SI, respectively (*12*). In the Ni-C state, the bridging ligand was shown to be a formal hydride (H^-) (*9*, *13*, *14*) which is supported by DFT calculations (*15*−*17*). For the diamagnetic states Ni-SI and Ni-R, direct spectroscopic evidence for the ligand's identity is lacking.

For *D. vulgaris* Miyazaki F [NiFe] hydrogenase, the redox states of the [NiFe] center have not been characterized by FTIR spectroscopy. The most complete data sets for a [NiFe] hydrogenase are available for *A. vinosum* (*18*), *D. gigas* (*12*), and *Desulfovibrio fructosovorans* (*19*). The FTIR spectra show a characteristic set of three bands in a spectral region between 1900 and 2200 cm^{-1}, which stem from the three

[†] This work was supported by Max Planck Society and European Union NEST-STREP RES 516510 (SOLAR-H).

* To whom correspondence should be addressed. E-mail: lubitz@mpi-muelheim.mpg.de. Telephone: +49(0)208-3063614. Fax: +49-(0)208-3063955.

[1] Abbreviations: FTIR, Fourier transform infrared; EPR, electron paramagnetic resonance; ENDOR, electron nuclear double resonance; OTTLE, optically transparent thin layer electrochemical (cell); MV, methyl viologen.

10.1021/bi0602462 CCC: $33.50
Published on Web 07/25/2006

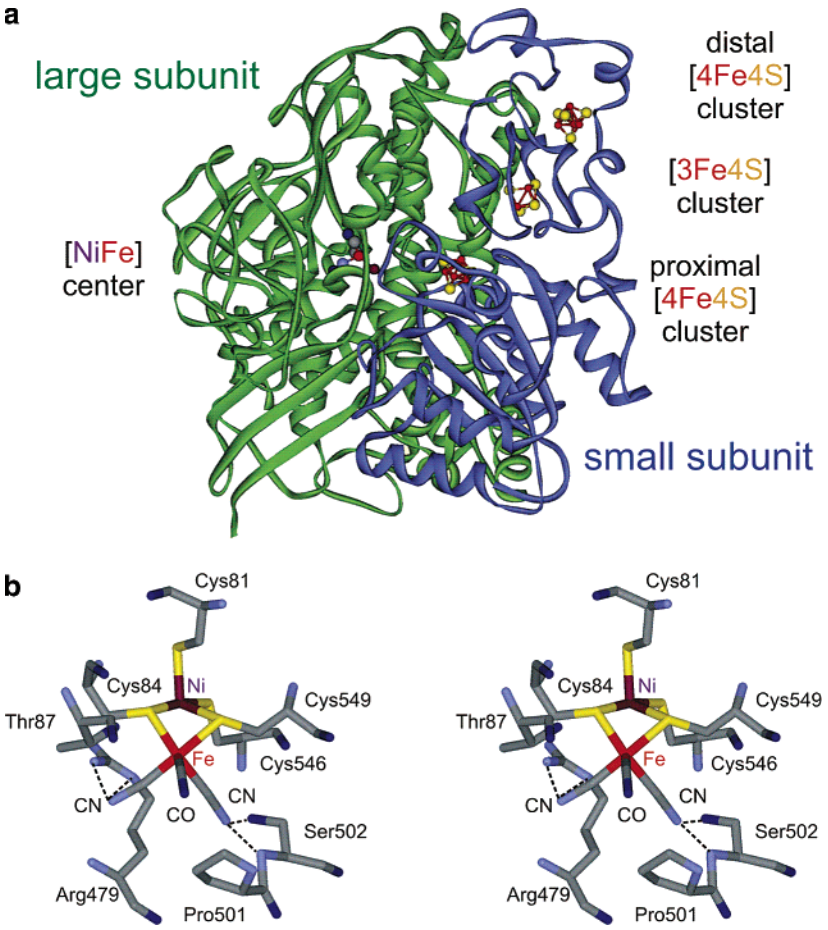

FIGURE 1: X-ray structure (resolution of 1.4 Å) of [NiFe] hydrogenase of *D. vulgaris* Miyazaki F in the reduced state [PDB entry 1H2R (*3*)]. (a) Overview of the protein showing the two subunits, the [NiFe] active site, and the three [FeS] clusters. (b) Stereoview of the active site including the amino acids which interact with the Fe ligands. Arg479 and Ser502 form H bonds to the CN^- ligands, whereas the CO ligand is connected to Pro501 and Thr87 via van der Waals interactions. Note that a third bridging ligand between Ni and Fe (oxygen- or sulfur-based) is present in the oxidized enzyme (*2*) that is missing here in the reduced state of the hydrogenase.

inorganic ligands to Fe. By means of ^{13}C and ^{15}N isotope labeling and a chemical analysis, these absorption bands were assigned to one CO molecule and two CN^- molecules (*6*, *20*). Because the IR spectra of *D. gigas* and *D. fructosovorans* [NiFe] hydrogenase look very similar to those of *A. vinosum* hydrogenase, De Lacey et al. (*12*, *19*) identified the three diatomic Fe ligands found in the crystal structure of these enzymes as one CO molecule and two CN^- molecules as well. For the [NiFe] hydrogenase of *D. vulgaris* Miyazaki F, only one FTIR spectrum has been published for the "as-isolated" state (a mixture of oxidized states Ni-A and Ni-B) (*21*). It consists of five bands, three of which are in the region of 2100−2050 cm^{-1} and two of which are in the region of 1960−1900 cm^{-1}. Though the spectrum resembles those of the [NiFe] hydrogenases of *A. vinosum*, *D. gigas*, and *D. fructosovorans*, one of the inorganic ligands was proposed to be a SO molecule (*21*).

In this work, we first address the question of the identity of the Fe ligands in the [NiFe] hydrogenase of *D. vulgaris* Miyazaki F by analyzing the FTIR spectra. We combine the FTIR method with electrochemistry, which allows us to study the FTIR spectra as a function of the potential applied to the spectroelectrochemical cell. This method can be advantageously used to optimize the presence of a particular redox state and to determine the midpoint potential of the redox transitions of the [NiFe] center (*12*, *18*). By the analysis of the pH dependence of the midpoint potentials, we were able to determine the p*K* values of the different transitions, for which it was found that each electronic transition is coupled to the transfer of one proton. Moreover, the diamagnetic EPR-silent states Ni-SU, Ni-SI, and Ni-R which are inaccessible to standard EPR spectroscopy have been investigated. We compare the FTIR frequencies of the bands in the spectra to those known for other [NiFe] hydrogenases and examine the similarities and differences. Finally, conclusions about the electronic configurations of the redox intermediates are drawn on the basis of the observed shifts of the vibrational frequencies of the Fe ligands.

EXPERIMENTAL PROCEDURES

Sample Preparation. D. vulgaris Miyazaki F was cultivated in a 50 L steel fermenter for 2 days. The hydrogenase was purified as described previously (*22*). Samples of 25 μL and 1.5 mM enzyme in 25 mM Tris-HCl and 100 mM KCl at different pHs were prepared. The pH of the enzyme solution was changed by first diluting the enzyme 10-fold with an appropriate buffer and then concentrating it to the starting volume using a Centricon YM50 concentrator (Millipore). This procedure was repeated 10 times.

For the spectroelectrochemical experiments, the enzyme was mixed with 10 different redox mediators to give a final

concentration of 125 μM for each. The following redox mediators were used (midpoint potentials E_m are given for pH 7 and 25 °C versus the normal hydrogen electrode): dichlorophenolindophenol, E_m = 220 mV (Sigma); 1,2-naphthoquinone, E_m = 145 mV (Sigma); phenazinemethosulfate, E_m = 80 mV (Sigma); methylene blue, E_m = 13 mV (Acros); indigo trisulfonate, E_m = −80 mV (Acros); indigo disulfate, E_m = −125 mV (Acros); anthraquinone-2-sulfonate, E_m = −230 mV (Sigma); phenosafranin, E_m = −252 mV (Acros); neutral red, E_m = −325 mV (Merck); and methyl viologen, E_m = −448 mV (Acros).

To optimize the Ni-A and Ni-SU states, the enzyme solution containing the redox mediators was pretreated in a gastight glass vessel as follows. The hydrogenase was added to an open Eppendorf tube into which a small magnetic stirring bar was introduced. The Eppendorf tube was inserted into the glass vessel containing 1 mL of buffer, and the glass vessel was closed with a gastight rubber stopper fixed by an aluminum ring. The enzyme was stirred gently and activated for 10 min at 37 °C with 100% H_2 gas, which was led into the glass vessel via a thin needle after evacuation of the vessel with a membrane pump. The hydrogen was then exchanged against CO by first removing the hydrogen by evacuation and then flushing the glass vessel with CO gas. The enzyme was incubated in a CO atmosphere for 10 min at room temperature. Finally, the hydrogenase was oxidized by removing the CO from the glass vessel and allowing air slowly to diffuse into the vessel via a thin needle. The oxidation was performed for 3 min at room temperature, and then the solution was stored on ice (10−15 min), until it was added to the spectroelectrochemical cell for measurement. This procedure has the drawback in that ∼40% of the protein is lost. The optimum pH value at which the largest amount of Ni-A/Ni-SU was obtained was 6.0.

All other states were generated electrochemically by first reducing the enzyme for 30 min at −500 mV. Then the optimum potential for the respective redox states was applied.

FTIR Spectroscopy. The experiments were performed on a Bruker IFS 66v/S FTIR spectrometer equipped with a HgCdTe (MCT) detector (Kolmar technologies). The sample chamber was flushed with dry air to minimize the contribution of water vapor. The spectral resolution was 2 cm^{-1}; the spectra were obtained at a scanner velocity of 20 kHz. Each spectrum was recorded in 5 min (200 scans). The optical path length of the FTIR cell is 8.5 μm (thickness of the gold mesh working electrode).

FTIR Spectroelectrochemistry. Enzyme solutions were subjected to different applied potentials using an optically transparent thin-layer electrochemical (OTTLE) cell with two CaF_2 windows as described by Moss et al. (*23*). The cell allows the electrochemical modification of the redox state of the enzyme directly in the IR cuvette using a gold mesh (55% transmission) as a working electrode, a platinum counter electrode, and a Ag/AgCl reference electrode. The electrodes were connected to a potentiostat (EG&G, type 283) which controls the potential and allows us to monitor the current during the measurements. The temperature was controlled by a thermostat (RML 6, Lauda) connected to the cell by a water circulation system. The thermostated spectroelectrochemical cell was directly mounted into the FTIR spectrometer. The measurements were performed at 30 °C in the case of the Ni-B, Ni-SI, Ni-C, and Ni-R redox states and at 15 °C in the case of the Ni-A and Ni-SU states. Electrochemical equilibration was attained when the current had reached a constant value (usually 5−7 min after the potential had been switched on). Recording of the FTIR spectra was therefore started ∼10 min after the potential was set.

The spectra were measured against the buffer solution as a background. A water vapor spectrum of suitable intensity was subtracted to correct for water vapor differences of the background and the sample spectra. Finally, a baseline correction was performed by subtracting a broad and structureless feature resembling the background. The reference electrode was calibrated using methyl viologen (MV) as a standard. Its first reduction potential was determined by square wave voltammetry with the same reference electrode and buffer that were used with the respective hydrogenase sample (25 mM Tris-HCl and 100 mM KCl at different pHs). An E'_0 value of −448 mV against a normal hydrogen electrode (NHE) was adopted for the reduction potential of the $MV^{2+}/MV^{\bullet+}$ redox couple (*24*). The potential difference between the observed potential value found in the calibration assay and −448 mV was used to calculate the applied potentials against the NHE. All potentials quoted in this study are given versus the NHE.

RESULTS

FTIR Spectra. Figure 2 shows the FTIR spectra of the different redox states of the [NiFe] hydrogenase of *D. vulgaris* Miyazaki F which were obtained by applying the indicated potentials to the enzyme solution. It is seen in the spectra that the exact positions of the bands vary according to the applied potential. It is expected that an IR spectrum of a pure redox state consists of three characteristic bands of the inorganic ligands to Fe, one in the spectral region of 1900−1960 cm^{-1} and two in the region of 2050−2100 cm^{-1}. For example, in spectrum c, an almost pure redox state is obtained under oxidizing conditions, Ni-B, and the spectrum exhibits three bands at 2090, 2081, and 1955 cm^{-1}. At other potentials, under more reducing conditions, the FTIR spectrum generally consists of the contributions of more than one redox state. By following the appearance and disappearance of the bands in the spectra as a function of the applied potential, we could uniquely assign the frequencies of the bands to specific redox states. These assignments are summarized in Table 1.

The spectra of the Ni-A and Ni-SU states shown in panels a and b of Figure 2 exhibit a lower signal/noise ratio than the other states, which is related to the sample preparation. The spectra were recorded at 15 °C, since at higher temperatures an increasing level of formation of Ni-B and Ni-SI states becomes rapidly apparent. In case of the Ni-SI state, the appearance of two CO bands in the region of 1900−1960 cm^{-1} indicates the existence of two species, and for the Ni-R state, even three bands have been found in this region.

FTIR Spectra of the Two Ni-SI States. The spectroelectrochemical measurements were performed for the Ni-SI states at different pH values in the pH range of 5.4−8.0 (Figure 3). At pH 5.4, the spectrum is dominated by a band at 1943 cm^{-1} and two bands at 2075 and 2086 cm^{-1} (Figure 3a). With an increase in pH, these bands decrease in intensity,

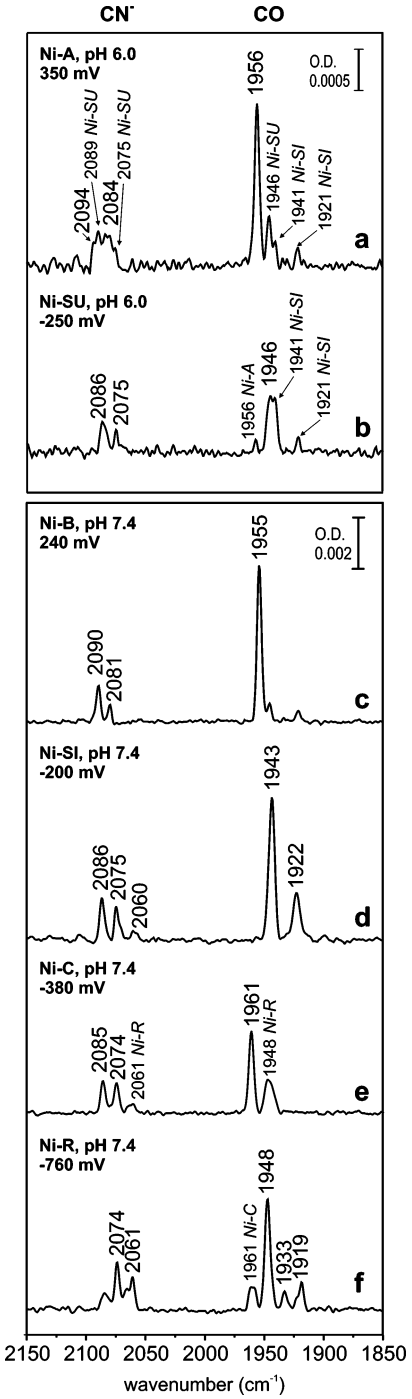

FIGURE 2: FTIR spectra of the different redox states of [NiFe] hydrogenase (1.5 mM in 25 mM Tris buffer with 100 mM KCl and each redox mediator at 125 μM). Each spectrum was obtained by accumulation of 200 scans. Spectra of states Ni-A (a) and Ni-SU (b) were recorded at 15 °C, and those of states Ni-B (c), Ni-SI (d), Ni-C (e), and Ni-R (f) were recorded at 30 °C. The applied potential, at which the respective state dominates, is indicated. The $\tilde{\nu}_{CO}$ and $\tilde{\nu}_{CN}$ vibrational frequencies are given for each state; bands of additionally occurring redox states (italics) are also given.

and three new bands, at 1922, 2056, and 2070 cm^{-1}, become more intense. At pH 7.8, the amplitudes of the bands at 1943 and 1922 cm^{-1} are almost equal (Figure 3d). These observations indicate that an acid−base equilibrium is present between the two Ni-SI states. The protonated form present at low pH values and characterized by vibrations at 1943, 2075, and 2086 cm^{-1} is called Ni-SIa according to De Lacey et al. (*12*), whereas the unprotonated form, Ni-SIr, present at high pH values exhibits absorption bands at 1922, 2056, and 2070 cm^{-1}. The pK_a value of this acid−base equilibrium for *D. vulgaris* Miyazaki F hydrogenase is 7.8 ± 0.1.

Table 1: Frequencies (wavenumbers, cm^{-1}) of the Bands in the IR Spectra of the [NiFe] Hydrogenase from *D. vulgaris* Miyazaki F in Different Redox States, Recorded at 30 °C and pH 7.4[a]

redox state	$\tilde{\nu}_{CO}$	$\tilde{\nu}_{CN}(1)$	$\tilde{\nu}_{CN}(2)$
Ni-A	1956	2084	2094
Ni-B	1955	2081	2090
Ni-SU	1946	2075	2086
Ni-SIr	1922	2056	2070
Ni-SIa	1943	2075	2086
Ni-C	1961	2074	2085
Ni-R	1948	2061	2074
Ni-R′	1919	2050	2065
Ni-R″	1933	nd[b]	nd[b]

[a] The error is ±1 cm^{-1}. The data were read from spectra as shown in Figures 2 and 3. Ni-SIa and Ni-SIr are the two states of Ni-SI which are in acid−base equilibrium (see text). Ni-R′ and Ni-R″ are substates of the most reduced state, Ni-R. The CN$^-$ bands of the Ni-R′ state were obtained from additional spectra (data not shown). [b] Not determined.

FTIR Spectra of the Three Ni-R States. The IR spectrum of the Ni-R state at pH 7.4 (Figure 2f) exhibits, in addition to the three predominant bands at 1948, 2061, and 2074 cm^{-1}, two additional bands at 1933 and 1919 cm^{-1}. In spectra at other pH values, corresponding bands at 2050 and 2065 cm^{-1} have been detected (data not shown; see Table 1). The fourth band at 1961 cm^{-1} results from that fraction of molecules which is still in the Ni-C state. Because the bands at 1933 and 1919 cm^{-1} were only detectable at very low potentials, they are assigned to the most reduced state, Ni-R. The appearance of these additional bands was investigated at different pH values in several independent measurements, but no dependence on pH could be detected within experimental error. They might therefore result from structurally different subforms of the Ni-R state (called Ni-R′ and Ni-R″). Unfortunately, it was not possible to substantially increase the intensity of these bands compared to those of the dominant Ni-R species. Additional peaks in the Ni-R state were also observed in other hydrogenases (*18*, *19*, *25*).

Potentiometric Titrations. The potentiometric titrations were performed to determine the midpoint potentials of the different redox transitions. The potential was scanned in the range from −600 to 200 mV in steps of 20−50 mV, and at each applied potential, an FTIR spectrum was recorded to monitor the spectral changes as a function of the potential. The peak height of the band in the region of 1900−1960 cm^{-1} (the CO band, vide infra) served as a probe for the analysis. The resulting data points were fitted to the Nernst equation:

$$E_h = E_m + \frac{RT}{nF} \times \ln\left(\frac{[ox]}{[red]}\right) \quad (1)$$

where E_h is the applied potential (millivolts), E_m is the midpoint potential (millivolts), R is the gas constant (8.314 J mol^{-1} K^{-1}), T is the temperature (K, Kelvin), n is the number of transferred electrons per protein molecule, F is the Faraday constant (96 485 C/mol) and [ox] and [red] are the concentrations of the oxidized and reduced species, respectively.

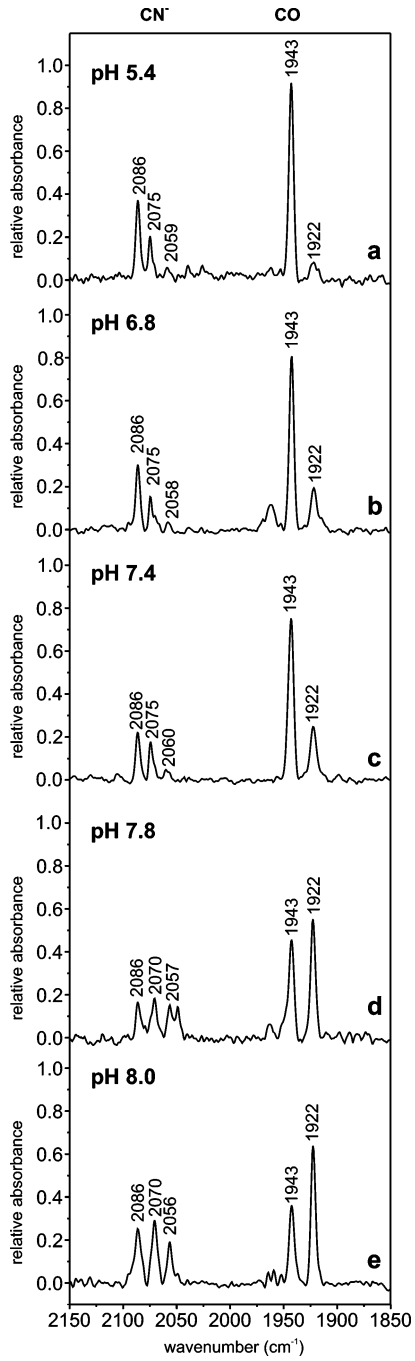

FIGURE 3: FTIR spectra of the two Ni-SI forms recorded at different pH values (1.5 mM in 25 mM Tris buffer with 100 mM KCl and each redox mediator at 125 μM). Each spectrum consists of 200 scans and was recorded at 30 °C. The spectra were normalized by setting the sum of the amplitudes of the two Ni-SI CO bands (1943 and 1922 cm^{-1}) to 1.0. Thus, the relative amplitude, which varies with pH, can be directly read from the spectrum. The spectra were recorded at the indicated potential for which the Ni-SI state dominated.

For the case in which electron transfer is accompanied by proton transfer, the midpoint potential in eq 1 is pH-dependent:

$$E_m = E_m(H^+) = E_m(\text{alk}) + \frac{RT}{nF} \times \ln\left(1 + \frac{[H^+]}{K_{red}}\right) \quad (2)$$

where E_m(alk) denotes the plateau value in the alkaline range and K_{red} the acid dissociation constant of the reduced form. At 30 °C and when pH < pK_{red}, the $E_m(H^+)$ value changes by −60 mV per pH unit for $n = 1$ and transfer of one proton (see Figure 5).

Figure 4 shows the titration curves at different pH values and the respective fits. Best fits were achieved by assuming a one-electron reaction for each redox transition ($n = 1$). The redox transition from Ni-A to Ni-SU was only obtained at pH 6, since no sufficient yield of the Ni-A state could be achieved at other pH values. In the case of the Ni-SI states, the sum of the bands of Ni-SIa and Ni-SIr was used. Thereby, it was assumed that the molar absorption coefficient is the same for both forms.

It is seen in Figure 4 that at very low and very high potentials the potentiometric titrations are not complete; i.e., the absorption bands of the redox couple present at these potentials did not fully reach 0 and 1, respectively. In these cases, a mixture of two states is present in the sample; e.g., in the case of the Ni-B state, the rest of the enzyme molecules always remained in the Ni-SI state. This stems from the fact that the mediators required to transport the electrons between the protein and the electrode are not able to completely reduce or oxidize the protein at extreme potentials. At potentials lower than −600 mV, the onset of protein degradation prevented the recording of reliable IR spectra because at this low potential proton reduction catalyzed by the hydrogenase interferes in the redox equilibrium. Thus, the determined midpoint potential is an apparent one. This also explains the large difference in potentials for the oxidative and reductive titrations.

Each redox titration was fully reversible, even at the low temperature of 5 °C (data not shown). This is different from the observations made for *A. vinosum* hydrogenase (*26*). Once the enzyme was activated by reducing an as-isolated sample at low potentials, only the Ni-B state was obtained after subsequent oxidation at potentials between 0 and 200 mV. A signal from the Ni-A state could not be detected. The activation (reduction of an as-isolated sample) and the inactivation (oxidation of a sample in the Ni-SI state) were finished within the electrochemical equilibration time of the OTTLE cell (5 min) even at temperatures as low as 5 °C (data not shown). This prevented a kinetic analysis. Also, in this respect, the results differ from those reported for *D. gigas* and *A. vinosum* hydrogenase in which inactivation (oxidation of Ni-SI to Ni-B) was hindered by a kinetic barrier and the Ni-B−Ni-SI redox titration was not reversible at low temperatures (2 and 5 °C, respectively) (*12*, *18*).

Each redox transition yielded two E_m values, one for the oxidative and one for the reductive titration. These two E_m values differed by a mean value of 6 ± 4 mV. The only exceptions were the Ni-C−Ni-R redox transitions at pH 6.8 and 8.0, where the two E_m values were determined to be 27 ± 4.5 and 18 ± 5.5 mV, respectively (see Figure 4c,f). This is related to the fact that at low potentials proton reduction additionally occurs and interferes in the redox equilibium. The midpoint potentials were taken as the average value of the two E_m values. They are collected in Table 2 and plotted versus pH in Figure 5 (top). From the figure, it is seen that the midpoint potentials decrease with an increase in pH. At higher pH values (>7.0), the experimental E_m values are almost constant with pH [see Figure 5 (top)].

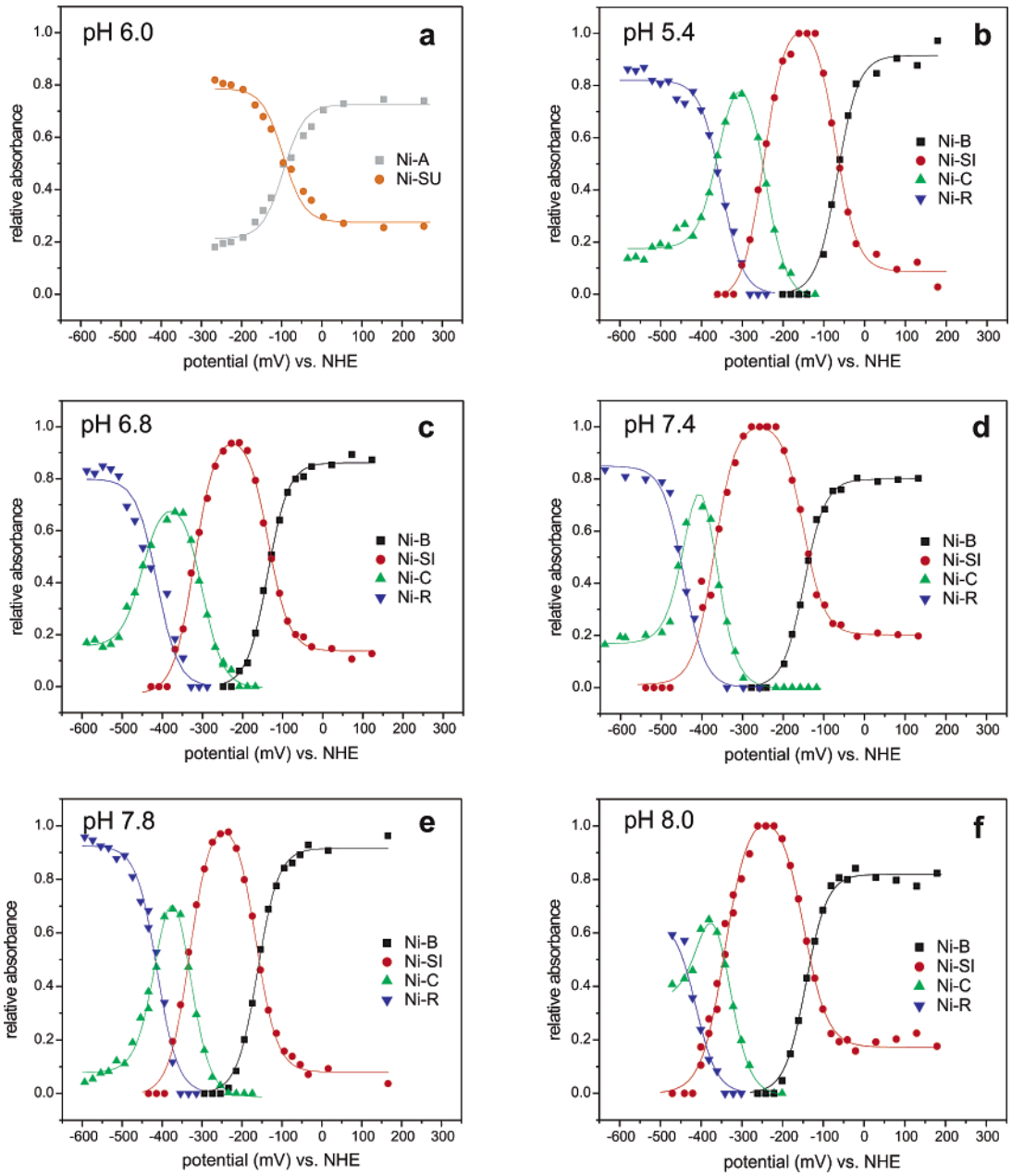

FIGURE 4: Determination of midpoint potentials of the different redox states. Each data point was extracted from a FTIR spectrum consisting of 200 scans measured at 15 °C in the case of the Ni-A−Ni-SU transition (a) and at 30 °C for all other transitions (b−f). The relative absorbance refers to the absorbance of the CO bands in each spectrum and is given against the applied potential. The sum of all CO absorbance bands in a spectrum is defined as 1.0. The part of a CO band representing a definite state is given relative to this value. The solid lines show the Nernst fits assuming $n = 1$ (correlation coefficient, $0.95 < R^2 < 0.99$). In panel a, only the Ni-A−Ni-SU transition is shown; no other transitions are included.

DISCUSSION

Assignment of the Fe Ligands. On the basis of the high degree of similarity of the spectra of *D. vulgaris* Miyazaki F enzyme with those of the homologous [NiFe] hydrogenases of *D. gigas* (*12*), *D. fructosovorans* (*19*), and *A. vinosum* (*18*), we identify the Fe ligands as one CO molecule and two CN^- molecules in *D. vulgaris* Miyazaki F. Higuchi et al. (*21*) explained the presence of two CN^- bands in the as-isolated sample with the presence of two redox states assuming that each state exhibits one CN^- band. The spectroelectrochemical measurements presented here clearly indicate that each state exhibits two bands in the CN^- region (Figure 2). As for the other [NiFe] hydrogenases investigated by IR spectroscopy, the third IR absorption band appears at frequencies around 1950 cm^{-1} and was assigned to a CO ligand. A SO molecule as one of the Fe ligands can be excluded on the basis of our data.

Comparison with Other [NiFe] Hydrogenases. In Figure 6, the frequencies of the bands in the IR spectrum of the different redox states of *D. vulgaris* Miyazaki F are compared with those of *D. gigas* and *A. vinosum*. The figure shows that the positions of the bands move in the same direction for all hydrogenases when the redox state is changed (the only exception is given by the Ni-A−Ni-SU transition). This indicates that the electronic structure of the active site and the redox processes that occur during the catalytic cycle are essentially the same in all these enzymes. The frequency of the CO bands in *D. vulgaris* Miyazaki F is systematically

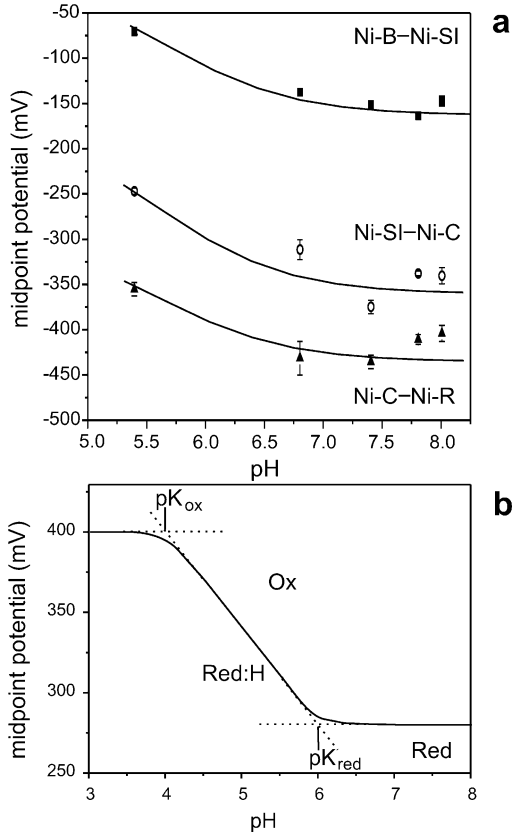

FIGURE 5: (a) Dependence of the midpoint potentials of the Ni-B−Ni-SI, Ni-SI−Ni-C, and Ni-C−Ni-R redox pairs on the pH value. The displayed curves are part of a curve describing a Pourbaix diagram (*49*) and show the character of such a dependence. (b) Theoretical diagram of a one-electron one-proton transition.

upshifted by ~10 cm^{-1} as compared to those of the other species, whereas the variation of the CN^- bands between the enzymes is limited to ≤2 cm^{-1} (Figure 6). The only exception seems to be the Ni-SU state (Figure 6). One can speculate that in *D. vulgaris* Miyazaki F this state differs significantly in its electronic configuration of the active site from that of the other organisms.

The position of the CO band can be influenced by molecules in the proximity of the CO ligand that interact through chemical bonds, hydrogen bonds, or van der Waals interaction. The CO ligand is surrounded by several uncharged amino acids, comprising a threonine (Thr87, large subunit) and a proline (Pro501, large subunit) (Figure 1). Comparison of the crystal structures of the *D. vulgaris* Miyazaki F enzyme (*2*) and the *D. gigas* enzyme (*25*) shows that of all amino acids within a radius of 5 Å around Ni only the two threonines, Thr80 and Thr87 (*D. vulgaris* amino acid numbering), are changed in *D. gigas* to an alanine and a valine, respectively. It is reported for the *D. fructosovorans* hydrogenase (*19*) (and *D. gigas* in which the amino acid sequence at these positions is the same as that for *D. fructosovorans*) that the valine is in van der Waals contact with the CO ligand. Since this unpolar residue is changed to a more polar threonine (Thr87; see Figure 1) in *D. vulgaris* Miyazaki F hydrogenase, the interaction is likely to be stronger. Nevertheless, the possible formation of a hydrogen bond between the OH group of Thr87 and the CO ligand is doubtful due to the rather large distance of 4.18 Å (hydroxyl-O_{Thr87}−$O_{CO\ ligand}$). However, the polarity of the threonine might cause an electron donation effect from the CO ligand toward the threonine compared to the effect of a valine which could explain the observed systematic frequency upshift of the absorbance band of the CO ligand.

Acid−Base Equilibrium of the Ni-SI States. The pH dependence of the ratio of the two Ni-SI forms reveals that they form an acid−base equilibrium in which Ni-SIa represents the protonated and Ni-SIr the unprotonated state. The pK_a value of the equilibrium was determined to be 7.8 ± 0.1. This value indicates that the proton-accepting base could be one of the coordinating cysteines since the pK value of the cysteine side chain (8.3) (*27*) is rather close to the measured value. Since the bridging cysteines are located closer to the Fe than the terminal cysteines, a protonation of one of the bridging cysteines seems to be more likely. On the other hand, a protonation of the OH^- bridging ligand which then leaves the active site as a water molecule would also be possible, as proposed for the *A. vinosum* hydrogenase (*18*, *28*, *29*). The frequency shifts of the CO and CN^- bands during the transition of the unprotonated to the protonated form (Table 1) are consistent with the decrease in electron density on Fe. Such an acid−base equilibrium was first reported for *D. gigas* hydrogenase and exhibited a similar pK value of 8 (*12*).

Subforms of the Ni-R State. Is was not possible to detect an acid−base equilibrium between the Ni-R state and its subforms in the [NiFe] hydrogenase of *D. vulgaris* Miyazaki F, since the ratio of their amplitudes was independent of the pH value in three measurement series. However, a pH dependence has been reported for *A. vinosum* hydrogenase (*18*), *D. fructosovorans* hydrogenase (*19*), and *D. gigas* hydrogenase (*30*). As the Ni-R′ subforms obviously do not differ in their protonation state in *D. vulgaris* Miyazaki F hydrogenase, the question concerning the nature of the active site in these states arises. The frequency shift could be due to a different structural organization of the active site and the surrounding amino acids. Another possible explanation has been discussed by Volbeda and Fontecilla-Camps (*31*), who raised the possibility that the different Ni-R states relate to different spin states of Ni^{II}. This is based on a DFT analysis of Ni-R with a hydride as the bridging ligand (*32*).

Midpoint Potentials of the Redox Transitions. The analysis of the titration curves yields the respective midpoint potentials of the various redox transitions between the states and shows that each reaction is a single-electron transition. Furthermore, the midpoint potentials depend on the pH, which indicates that each transition is accompanied by a change in the protonation state (see Figure 5). It is seen that the potentials are almost constant for pH >7 and become more positive toward lower pHs for pH <7. The slope between pH 5.4 and 6.0 is ~60 mV/pH, which fits well for a situation where oxidized and reduced species (Ox and Red:H, respectively) are unprotonated (Ox) and protonated (Red:H) by one proton, respectively. At pH >7, neither reduced nor oxidized species are protonated. Such pH dependence is described by eq 2.

Though the experimental data points do not cover the complete curve (see Figure 5), it is estimated that the pK_a value of the reduced forms for all three redox transitions lies between 6.5 and 7 with some small variations. The proton acceptor could thus be one of the four coordinating cysteines which would fit to the pK value of the thiol group (pK =

Table 2: Midpoint Potentials of Redox Pairs Observed in Redox Transitions of the *D. vulgaris* Miyazaki F [NiFe] Hydrogenase Measured at 30 °C[a]

species	pH	$E_m(H^+)$ (mV)			
		Ni-A−Ni-SU	Ni-B−Ni-SI	Ni-SI−Ni-C	Ni-C−Ni-R
D. vulgaris Miyazaki F	6.0	−96 ± 5			
	5.4		−69.5 ± 4.5	−246.5 ± 3.5	−355.5 ± 5.5
	6.8		−136.5 ± 0.5	−311.0 ± 11	−431.5 ± 18.5
	7.4		−150.5 ± 4.5	−374.5 ± 7.5	−435.5 ± 7.5
	7.8		−162.5 ± 3.5	−337.5 ± 2.5	−410.5 ± 5.5
	8.0		−146.5 ± 5.5	−340.0 ± 9	−404.0 ± 9
D. gigas (*18*, *38*)	8.0[b]	−120	−150	−380	−445
	8.0[c]		−140	−330	−405

[a] For comparison, the data for *D. gigas* [NiFe] hydrogenase are included (last two rows). [b] The data for *D. gigas* [NiFe] hydrogenase were derived from FTIR spectroscopy; the pH dependencies of the four transitions are −55, −36, −47, and −43 mV/pH unit (*12*). [c] These data for *D. gigas* [NiFe] hydrogenase were derived from EPR spectroscopy (*39*).

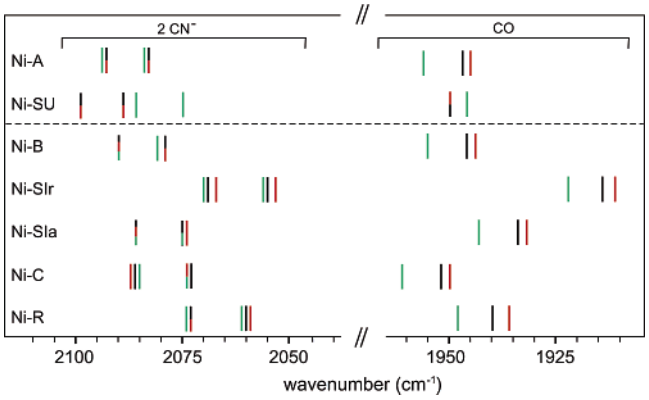

FIGURE 6: Overview of CO and CN^- vibrational bands measured for [NiFe] hydrogenases from *D. gigas* (black) (*12*), *A. vinosum* (red) (*18*), and *D. vulgaris* Miyazaki F (green).

8.3), taking into account the fact that the p*K* of an amino acid can change in the protein surrounding. Nevertheless, other amino acids such as glutamate or aspartate are possible proton acceptors as well, even if the tabulated p*K* values are 4.3 and 3.9, respectively (*27*). This is supported by a mutagenesis study of *D. fructosovorans* hydrogenase in which a glutamate, which is supposed to be related to the H^+ proton transfer path, was changed to a glutamine, leading to a decreased catalytic activity (*33*). Furthermore, the protons could be bound to the H-bond network of the protein (*31*).

Redox titrations on [NiFe] hydrogenases were performed not only via IR spectroscopy using the ligands bound to Fe as a probe but also via EPR spectroscopy by monitoring the change of the Ni signals, i.e., the disappearance of the Ni-A and Ni-B signal and the appearance and subsequent disappearance of the Ni-C signal during reduction of the protein (*34*−*39*). The midpoint potentials reported in these publications are similar to those determined for *D. vulgaris* Miyazaki F hydrogenase presented here (Table 2). They are similar to those obtained for the hydrogenases of *D. gigas* and *A. vinosum* by IR spectroelectrochemistry (*12*, *18*). In a manner independent of the method used to determine the midpoint potentials, it was shown for the different [NiFe] hydrogenases that with each redox transition one proton is transferred and each titration curve can be best fitted assuming a one-electron transition.

Electronic Configuration of the Different Redox States. The frequency shifts of the CO and CN^- bands with a change in the redox state largely depend on the change of the charge on the Fe ion which is related to the changes of the valence state of Ni, the redox-active metal. Since the CO and CN^- molecules possess π-electron accepting capabilities, they are able to sense changes in the electron density on Fe. This results in a shift of the IR frequencies because the back-donation effect from the Fe to the ligands becomes larger when the active site is reduced and vice versa, affecting the order of the Fe−C, C═O, and C≡N bonds (*40*).

During the redox transitions, the formal oxidation state switches between Ni^{III} and Ni^{II} (Figure 7). The Fe is believed to be always low-spin Fe^{II} ($S = 0$), since no substantial hyperfine structure of ^{57}Fe can be detected in the EPR/ENDOR spectra (*41*−*43*). Furthermore, for a charge of the Fe oxidation state, large shifts of the CO and CN^- vibrational bands would be expected (*44*). The smaller shifts in [NiFe] hydrogenases show that the Fe is not changing its formal oxidation state; it only senses effects from neighboring atoms (mainly Ni) leading to small shifts of the Fe electron density and the related CO and CN^- vibrations.

During the reduction of Ni-A to Ni-SU, the CO vibrational frequency shifts from 1956 to 1946 cm^{-1} (−10 cm^{-1}). The CN^- bands shift by approximately the same amount (Figures 2a,b and 6 and Table 1). Since a frequency downshift is associated with the increase in the Fe electron density affecting both the CO and CN^- ligands in the same way, it can be assumed that the Ni is reduced from Ni^{III} to Ni^{II}. Here the situation is different from what is reported for *D. gigas* [NiFe] hydrogenase in which the Ni-A−Ni-SU transition was associated with CO and CN^- frequency upshifts of 4 and 6 cm^{-1}, respectively (*12*), and it is unclear at present what causes the difference between the Ni-SU states in these enzymes.

In the case of the Ni-B−Ni-SIr redox transition, the frequency of the CO ligand is downshifted by −33 cm^{-1} (Figure 6 and Table 1), indicating an increase in the electron density on Fe. In Ni-B, the formal oxidation state of the Ni is Ni^{III} and an increase in the electron density on Fe is consistent with the formal reduction of Ni by one electron from Ni^{III} to Ni^{II}. The frequency shift of the CN^- ligands supports this assignment since they also shift to lower frequencies (Figure 6 and Table 1). Again, the change in the Ni oxidation state influences the CO and CN^- ligands in the same way but is slightly smaller for the CN^- ligands due to the better π-accepting ability of the CO molecule which leads to more pronounced electronic changes on Fe and CO ligand vibrations than for CN^- (*44*, *45*). During the

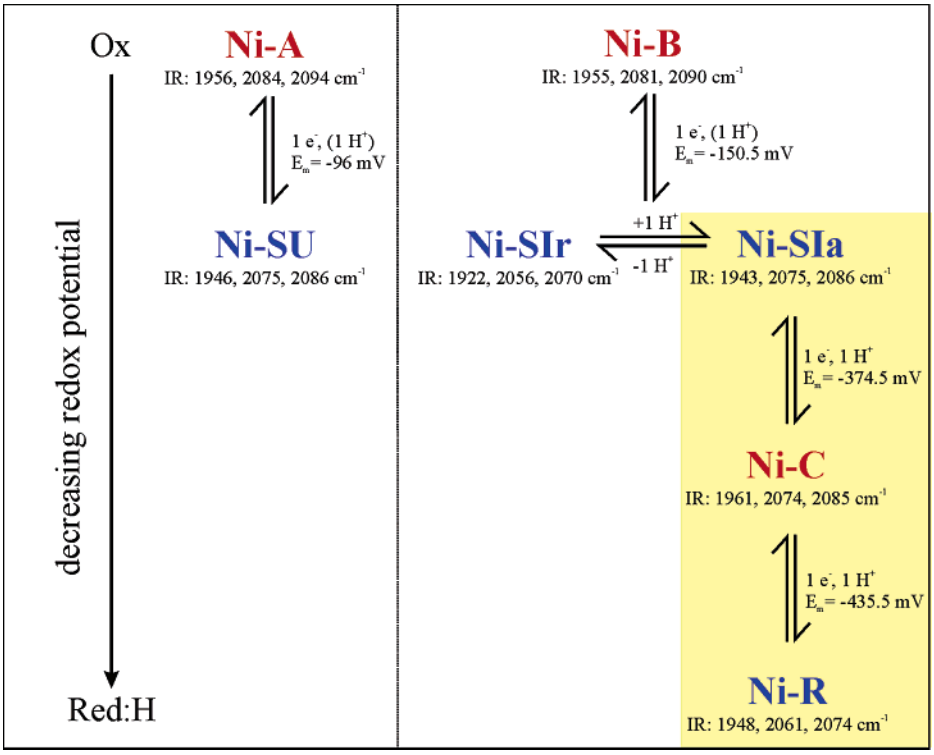

FIGURE 7: Schematic overview of the different redox states of *D. vulgaris* Miyazaki F hydrogenase summarizing the IR frequencies and redox chemistry of the active site. In the paramagnetic ($S = {}^1/_2$) states (Ni-A, Ni-B, and Ni-C), the Ni has a formal oxidation state of +3, whereas in the EPR-silent states, it is +2. The two Ni-SI forms are in an acid−base equilibrium. The midpoint potentials are given for pH 6 (Ni-A−Ni-SU) and for pH 7.4 (all other transitions). The states (from top to bottom) are ordered according to the decreasing redox potential. Note that the formal oxidation state of Ni in this process cycles from oxidized to reduced and back to oxidized before the fully reduced Ni-R state is reached (see the text).

reduction of an oxidized sample, the Ni-SIr state is first present. When the enzyme is further reduced, the Ni-SIa state develops and reaches a higher relative intensity than the Ni-SIr state before both Ni-SI states dissipate and the Ni-C state arises (data not shown). This result indicates that the Ni-SIr−Ni-SIa transition is required for the activation of the enzyme.

In the subsequent Ni-SIa−Ni-C transition, the frequency of the CO band is upshifted again (18 cm^{-1}) (Figure 6 and Table 1). It can thus be concluded that Ni is formally not further reduced to Ni^{I} but oxidized back to Ni^{III} since the frequency upshift suggests a decrease in the electron density on Fe caused by the oxidation of Ni. Furthermore, this transition includes the reduction of a proton to a formal hydride forming a bridge between Ni and Fe. The insertion of a formally negatively charged ligand (hydride) should lead to an increase in the electron density on Fe, resulting in a frequency downshift. As this transition shows a frequency upshift, the formation of the hydride bridge does not seem to strongly influence the shift. Strikingly, the frequency shifts of the CN^- ligands do not follow the CO frequency shift. It is inverted in the case of the Ni-SIa−Ni-C transition (−1 cm^{-1}) (Figure 6 and Table 1). This difference suggests that a possible deprotonation of a base (most likely a nearby amino acid) providing the proton for the formation of the hydride bridge especially affects the CN^- ligands, possibly caused by an increased negative partial charge on one of the interacting amino acids. This charge effect would result in an enhanced donation of electrons to the CN^- ligands which results in a frequency downshift. Such a downshift might be as strong as the frequency upshift caused by Ni oxidation resulting in a cancellation of the effect. The same effect was observed when the influence of the protonation of $K[\eta^5\text{-}(C_5H_5)FeCO(CN)_2]$ model complexes mimicking the active site of the enzyme was analyzed (*44*). A possible alternative is given by Volbeda and Fontecilla-Camps for the *D. gigas* hydrogenase which shows the same effect (*31*) in that they relate it to the trans effect of the bridging hydride acting on the Fe−CO bond: The CO group and the H^- molecule share the same metal orbital which leads to a weakened Fe−C bond and a strengthened C═O bond.

In the Ni-C−Ni-R transition, another reduction (Ox → Red:H) takes place (Figures 6 and 7 and Table 1). The reduction again causes an increase in the electron density at Fe manifested in the downshift of the CO as well as the CN^- frequency by approximately 13 cm^{-1}.

The relationship between the different redox states as proposed in this work (Figure 7) is in general agreement with those published for other [NiFe] hydrogenases with only minor variations. Bleijlevens et al. described for *A. vinosum* three different forms of Ni-SI, two of which are spectroscopically identical but differ in their activity (*18*). The presence of an inactive form of Ni-SIa in *D. vulgaris* Miyazaki F was not detected since even at low temperatures (5 °C) an activation to the Ni-C and Ni-R states was easily possible. Most of the measurements were performed at 30 °C at which a fast activation takes place. The same explanation was given for the *D. gigas* enzyme, for which at 40 °C no inactive Ni-SIa state was discovered (*12*). The activation step between the Ni-SU and Ni-SI states, which was determined by following the Ni-SU kinetics during the electrochemical reduction of an as isolated sample of *D.*

gigas (*12*, *46*), was not examined in *D. vulgaris* Miyazaki F hydrogenase, since the Ni-SU state was not detectable in an as-isolated sample. Moreover, the observed frequency shifts are in line with several proposed reaction mechanisms (*18*, *32*, *47*) but cannot give any experimental preference for one of them. Here more experimental and theoretical data are needed to come to a conclusion.

CONCLUSION

In this work, we have presented a detailed FTIR spectroscopic study of the different redox intermediates of the [NiFe] hydrogenase of *D. vulgaris* Miyazaki F. It was shown that the Fe carries one CO molecule and two CN^- molecules as ligands as found for *D. gigas* and *A. vinosum* hydrogenase, demonstrating the high degree of similarity among these three enzymes. A further similarity concerns the redox transitions which are accompanied by a single proton transfer step and the observed acid−base equilibrium of the Ni-SI states that possess a very similar p*K* value. It is tempting to speculate that the pH dependence of the Ni-SIr−Ni-SIa transition indeed involves a protonation of the bridging OH^- ligand that must be removed before the enzyme becomes active (*18*, *28*, *48*). The removal of water from the active site in the different enzymes seems to require a different activation energy which is higher in *A. vinosum* (*18*) and *D. gigas* (*12*) than in *D. vulgaris* Miyazaki F.

Other differences between the enzymes have been observed. A systematic frequency shift of the CO band in all states is probably due to a difference in the amino acid surrounding of the active site in *D. vulgaris* Miyazaki F compared with that in *D. gigas*. Furthermore, no pH dependence of the Ni-R substates could be observed. It could therefore be that the Ni-R′ forms are non-native states representing slightly different conformations or spin states of the enzyme. The band shifts in the IR spectrum with a change in the pH of the redox titrations yielded the p*K* values of the reactions. The protonation steps in the redox transitions probably involve addition of H^+ to one of the four cysteine residues coordinating the active site, but a protonation of other residues cannot be excluded at present. The frequency shifts of the CO and CN^- groups have been related to the change in the formal oxidation state of Ni, switching between Ni^{III}, with higher $\tilde{\nu}_{CO}$ IR frequencies, and Ni^{II}, with lower frequencies. Nevertheless, further experiments need to be performed to gain more detailed insight into the catalytic cycle as well as the sites of protonation in the protein near the active site. This could be achieved by studying appropriate site-directed mutants of the [NiFe] hydrogenase of *D. vulgaris* Miyazaki F. Such experiments are underway in our laboratory.

ACKNOWLEDGMENT

We gratefully acknowledge the technical assistance of Tanja Berndsen in preparing the [NiFe] hydrogenase, Leslie Currell for his support with the FTIR measurements, and Maurice van Gastel for helpful discussions and careful revision of the manuscript.

REFERENCES

1. Adams, M. W. W., Mortenson, L. E., and Chen, J.-S. (1981) Hydrogenase, *Biochim. Biophys. Acta 594*, 105−176.
2. Higuchi, Y., Yagi, T., and Yasuoka, N. (1997) Unusual ligand structure in Ni-Fe active center and an additional Mg site in hydrogenase revealed by high-resolution X-ray structure analysis, *Structure 5*, 1671−1680.
3. Higuchi, Y., Ogata, H., Miki, K., Yasuoka, N., and Yagi, T. (1999) Removal of the bridging ligand atom at the Ni-Fe active site of [NiFe] hydrogenase upon reduction with H_2, as revealed by X-ray structure analysis at 1.4 Å resolution, *Structure 7*, 549−556.
4. Ogata, H., Mizogushi, Y., Mizuno, N., Miki, K., Adachi, S., Yasuoka, N., Yagi, T., Yamauchi, O., Hirota, S., and Higuchi, Y. (2002) Structural studies of the carbon monoxide complex of [NiFe] hydrogenase from *Desulfovibrio vulgaris* Miyazaki F: Suggestion for the initial activation site for dihydrogen, *J. Am. Chem. Soc. 124*, 11628−11635.
5. Ogata, H., Hirota, S., Nakahara, A., Komori, H., Shibata, N., Kato, T., Kano, K., and Higuchi, Y. (2005) Activation process of [NiFe] hydrogenase elucidated by high resultion X-ray analysis: Conversion of the ready to unready state, *Structure 13*, 1635−1642.
6. Happe, R. P., Roseboom, W., Pierik, A. J., Albracht, S. P. J., and Bagley, K. A. (1997) Biological activation of hydrogen, *Nature 385*, 126.
7. Fernandez, V. M., Hatchikian, E. C., and Cammack, R. (1985) Properties and reactivation of two different deactivated forms of *Desulfovibrio gigas* hydrogenase, *Biochim. Biophys. Acta 832*, 69−79.
8. van Gastel, M., Fichtner, C., Neese, F., and Lubitz, W. (2005) EPR experiments to elucidate the structure of the ready and unready states of the [NiFe] hydrogenase of *Desulfovibrio vulgaris* Miyazaki F, *Biochem. Soc. Trans. 33*, 7−11.
9. Foerster, S., Stein, M., Brecht, M., Ogata, H., Higuchi, Y., and Lubitz, W. (2003) Single-crystal EPR studies of the reduced active site of [NiFe] hydrogenase from *Desulfovibrio vulgaris* Miyazaki F, *J. Am. Chem. Soc. 125*, 83−93.
10. van Gastel, M., Stein, M., Brecht, M., Schröder, O., Lendzian, F., Bittl, R., Ogata, H., Higuchi, Y., and Lubitz, W. (2006) A single-crystal ENDOR and density functional theory study of the oxidized states of the [NiFe] hydrogenase from *Desulfovibrio vulgaris* Miyazaki F, *J. Biol. Inorg. Chem. 11*, 41−51.
11. Volbeda, A., Martin, L., Cavazza, C., Matho, M., Faber, B. W., Roseboom, W., Albracht, S. P. J., Garcin, E., Rousset, M., and Fontecilla-Camps, J. C. (2005) Structural difference between the ready and unready oxidized states of [NiFe] hydrogenases, *J. Biol. Inorg. Chem. 10*, 239−249.
12. De Lacey, A. L., Hatchikian, E. C., Volbeda, A., Frey, M., Fontecilla-Camps, J. C., and Fernandez, V. M. (1997) Infrared-spectroelectrochemical characterization of the [NiFe] hydrogenase of *Desulfovibrio gigas*, *J. Am. Chem. Soc. 119*, 7181−7189.
13. Foerster, S., van Gastel, M., Brecht, M., and Lubitz, W. (2005) An orientation-selected ENDOR and HYSCORE study of the Ni-C active state of *Desulfovibrio vulgaris* Miyazaki F hydrogenase, *J. Biol. Inorg. Chem. 10*, 51−62.
14. Brecht, M., van Gastel, M., Buhrke, T., Friedrich, B., and Lubitz, W. (2003) Direct detection of a hydride ligand in the [NiFe] center of the regulatory hydrogenase from *Ralstonia eutropha* in its reduced state by HYSCORE and ENDOR spectroscopy, *J. Am. Chem. Soc. 125*, 13075−13083.
15. Niu, S., Thomson, L. M., and Hall, M. B. (1999) Theoretical characterization of the reaction intermediates in a model of the nickel−iron hydrogenase of *Desulfovibrio gigas*, *J. Am. Chem. Soc. 121*, 4000−4007.
16. Stein, M., van Lenthe, E., Baerends, E. J., and Lubitz, W. (2001) Relativistic DFT calculations of the paramagnetic intermediates of the [NiFe] hydrogenase. Implications for the enzymatic mechanism, *J. Am. Chem. Soc. 123*, 5839−5840.
17. Pavlov, M., Siegbahn, P. E. M., Blomberg, M. R. A., and Crabtree, R. H. (1998) Mechanism of H−H activation by nickel−iron hydrogenase, *J. Am. Chem. Soc. 120*, 548−555.
18. Bleijlevens, B., van Broekhuizen, F., De Lacey, A. L., Roseboom, W., Fernandez, V. M., and Albracht, S. P. J. (2004) The activation of the [NiFe]-hydrogenase from *Allochromatium vinosum*. An infrared spectro-electrochemical study, *J. Biol. Inorg. Chem. 9*, 743−752.
19. De Lacey, A. L., Stadler, C., Fernandez, V. M., Hatchikian, E. C., Fan, H. J., Li, S., and Hall, M. B. (2002) IR spectroelectrochemical study of the binding of carbon monoxide to the active site of *Desulfovibrio fructosovorans* Ni-Fe hydrogenase, *J. Biol. Inorg. Chem. 7*, 318−326.
20. Pierik, A. J., Roseboom, W., Happe, R. P., Bagley, K. A., and Albracht, S. P. J. (1999) Carbon monoxide and cyanide as intrinsic

ligands to iron in the active site of [NiFe]-hydrogenases: NiFe-$(CN)_2CO$, biology's way to activate H_2, *J. Biol. Chem. 274*, 3331−3337.
21. Higuchi, Y., Toujou, F., Tsukamoto, K., and Yagi, T. (2000) The presence of a SO molecule in [NiFe] hydrogenase from *Desulfovibrio vulgaris* Miyazaki as detected by mass spectrometry, *J. Inorg. Biochem. 80*, 205−211.
22. Yagi, T., Kimura, K., Daidoji, H., Sakai, F., Tamura, S., and Inokuchi, H. (1976) Properties of purified hydrogenase from the particulate fraction of *Desulfovibrio vulgaris* Miyazaki, *J. Biochem. 79*, 661−671.
23. Moss, D., Nabedryk, E., Breton, J. L. J., and Mäntele, W. (1990) Redox-linked conformational changes in proteins detected by a combination of infrared spectroscopy and protein electrochemistry, *Eur. J. Biochem. 187*, 565−572.
24. Wardman, P. (1989) Reduction potentials of one-electron couples involving free radicals in aqueous solution, *J. Phys. Chem. Ref. Data 18*, 1637−1755.
25. Volbeda, A., Garcin, E., Piras, C., De Lacey, A. L., Fernandez, V. M., Hatchikian, E. C., Frey, M., and Fontecilla-Camps, J. C. (1996) Structure of the [NiFe] hydrogenase active site: Evidence for biologically uncommon Fe ligands, *J. Am. Chem. Soc. 118*, 12989−12996.
26. Coremans, J. M. C. C., van der Zwaan, J. W., and Albracht, S. P. J. (1992) Distinct redox behaviour of the prosthetic groups in ready and unready hydrogenase from *Chromatium vinosum*, *Biochim. Biophys. Acta 1119*, 157−168.
27. Stryer, L. (1975) *Biochemistry*, W. H. Freeman and Company, San Francisco.
28. Kurkin, S., George, S. J., Thorneley, R. N. F., and Albracht, S. P. J. (2004) Hydrogen-induced activation of the [NiFe]-hydrogenase from *Allochromatium vinosum* as studied by stopped-flow infrared spectroscopy, *Biochemistry 43*, 6820−6831.
29. Vincent, K. A., Cracknell, J., Parkin, A., and Armstrong, F. A. (2005) Hydrogen cycling by enzymes: Electrocatalysis and implications for future energy technology, *Dalton Trans*., 3397−3403.
30. De Lacey, A. L., Pardo, A., Fernandez, V. M., Dementin, S., Adryanczyk-Perrier, G., Hatchikian, E. C., and Rousset, M. (2004) FTIR spectroelectrochemical study of the activation and inactivation processes of [NiFe] hydrogenases: Effects of solvent isotope replacement and site-directed mutagenesis, *J. Biol. Inorg. Chem. 9*, 636−642.
31. Volbeda, A., and Fontecilla-Camps, J. C. (2005) Structure−function relationship of nickel−iron sites in hydrogenase and a comparison with the active site of other nickel−iron enzymes, *Coord. Chem. Rev. 249*, 1609−1619.
32. Bruschi, M., De Gioia, L., Zampalla, G., Reiher, M., Fantucci, P., and Stein, M. (2004) A theoretical study of spin states in Ni−S_4 complexes and models of the [NiFe] hydrogenase active site, *J. Biol. Inorg. Chem. 9*, 873−884.
33. Dementin, S., Burlat, B., De Lacey, A. L., Pardo, A., Adryanczyk-Perrier, G., Guigliarelli, B., Fernandez, V. M., and Rousset, M. (2004) A glutamate is the essential proton transfer gate during the catalytic cycle of the [NiFe] hydrogenase, *J. Biol. Chem. 279*, 10508−10513.
34. Teixeira, M., Moura, I., Xavier, A. V., DerVartanian, D. V., LeGall, J., Peck, H. D., Jr., Huynh, B. H., and Moura, J. J. G. (1983) *Desulfovibrio gigas* hydrogenase: Redox properties of the nickel and iron−sulfur centers, *Eur. J. Biochem. 130*, 481−484.
35. Teixeira, M., Moura, I., Xavier, A. V., Huynh, B. H., DerVartanian, D. V., Peck, H. D., Jr., LeGall, J., and Moura, J. J. G. (1985) Electron paramagnetic resonance studies on the mechanism of activation and the catalytic cycle of the nickel-containg hydrogenase from *Desulfovibrio gigas*, *J. Biol. Chem. 260*, 8942−8950.
36. Fernandez, V. M., Hatchikian, E. C., Patil, D. S., and Cammack, R. (1986) ESR-detectable nickel and iron-sulphur centres in relation to the reversible activation of *Desulfovibrio gigas* hydrogenase, *Biochim. Biophys. Acta 883*, 145−154.
37. Cammack, R., Patil, D. S., Hatchikian, E. C., and Fernandez, V. M. (1987) Nickel and iron-sulphur centres in *Desulfovibrio gigas* hydrogenase: ESR spectra, redox properties and interaction, *Biochim. Biophys. Acta 912*, 98−109.
38. Teixeira, M., Moura, I., Xavier, A. V., Moura, J. J. G., LeGall, J., DerVartanian, D. V., Peck, H. D., Jr., and Huynh, B. H. (1989) Redox intermediates of *Desulfovibrio gigas* [NiFe] hydrogenase generated under hydrogen. Mössbauer and EPR characterization of the metal centers, *J. Biol. Chem. 264*, 16435−16450.
39. Roberts, L. M., and Lindahl, P. A. (1995) Stoichiometric reductive titrations of *Desulfovibrio gigas* hydrogenase, *J. Am. Chem. Soc. 117*, 2565−2572.
40. Volbeda, A., and Fontecilla-Camps, J. C. (2003) The active site and catalytic mechanism of NiFe hydrogenases, *Dalton Trans. 21*, 4030−4038.
41. Huyett, J. E., Carepo, M., Pamplona, A., Franco, R., Moura, I., Moura, J. J. G., and Hoffman, B. M. (1997) ^{57}Fe Q-band pulsed ENDOR of the hetero-dinuclear site of nickel hydrogenase: Comparison of the NiA, NiB, and NiC states, *J. Am. Chem. Soc. 119*, 9291−9292.
42. Fan, C., Teixeira, M., Moura, J. J. G., Moura, I., Huynh, B. H., LeGall, J., Peck, H. D., Jr., and Hoffman, B. M. (1991) Detection and characterisation of exchangeable protons bound to the hydrogen-activation nickel site of *Desulfovibrio gigas* hydrogenase: A proton and deuterium Q-band ENDOR study, *J. Am. Chem. Soc. 113*, 20−24.
43. Dole, F., Fournel, A., Magro, V., Hatchikian, E. C., Bertrand, P., and Guigliarelli, B. (1997) Nature and electronic structure of the Ni-X dinuclear center of *Desulfovibrio gigas* hydrogenase. Implications for the enzymatic mechanism, *Biochemistry 36*, 7847−7854.
44. Darensbourg, M. Y., Lyon, E. J., and Smee, J. (2000) The bio-organometallic chemistry of active site iron in hydrogenases, *Coord. Chem. Rev. 206−207*, 533−561.
45. Lai, C.-H., Lee, W.-Z., Miller, M. L., Reibenspies, J. H., Darensbourg, D. J., and Darensbourg, M. Y. (1998) Responses of the $Fe(CN)_2(CO)$ Unit to electronic changes as related to its role in [NiFe] hydrogenase, *J. Am. Chem. Soc. 120*, 10103−10114.
46. De Lacey, A. L., Fernandez, V. M., and Rousset, M. (2005) Native and mutant nickel−iron hydrogenases: Unravelling structure and function, *Coord. Chem. Rev. 249*, 1596−1608.
47. Stein, M., and Lubitz, W. (2004) Relativistic DFT calculations of the reaction cycle intermediates of [NiFe] hydrogenase: A contribution to understanding the enzymatic mechanism, *J. Inorg. Biochem. 98*, 862−877.
48. Lamle, S. E., Albracht, S. P. J., and Armstrong, F. A. (2005) The mechanism of activation of a [NiFe]-hydrogenase by electrons, hydrogen, and carbon monoxide, *J. Am. Chem. Soc. 127*, 6595−6604.
49. Bailey, S. I., Ritchie, I. M., and Hewgill, F. R. (1983) The construction and use of potential-pH diagrams in organic oxidation−reduction reactions, *J. Chem. Soc., Perkin Trans 2*, 645−652.

BI0602462